DEVELOPMENTAL BIOLOGY 171, 317–329 (1995)

A Transgenic Neuroanatomical Marker Identifies Cranial Neural Crest Deficiencies Associated with the *Pax3* Mutant *Splotch*

Patrick Tremblay, Michael Kessel, and Peter Gruss[1]

Abteilung für Molekulare Zellbiologie, Max-Planck-Institut für Biophysikalische Chemie, Am Fassberg, D-37077 Göttingen, Germany

The murine *Pax3* gene encodes a transcription factor containing a paired domain as well as a paired-type homeodomain. Its expression during embryonic development is temporally and spatially restricted, including mainly the dorsal part of the neural tube, the mesencephalon, the neural crest derivatives, and the dermomyotome. Development in the absence of *Pax3* can be studied in *Splotch* mutant mice, which bear mutations within the *Pax3* gene. Various alleles have been phenotypically and molecularly characterized. Abnormalities have been observed in the brain, the neural tube, the trunk neural crest derivatives and in muscles of these mutants. The importance of *PAX3* during human embryonal development is readily seen in Waardenburg patients, who present a dominant inherited syndrome consisting mainly of craniofacial abnormalities, pigmentation deficiencies, and deafness, consecutive to *PAX3* mutations. In order to analyze the nervous system of *Splotch* embryos in more detail, we employed the transgenic mouse line L17. These transgenic mice harbor a β-galactosidase marker gene under the control of Hoxa-7 promoter elements. Probably in combination with *cis*-elements adjacent to the integration site of the L17 transgene, the Hoxa-7 elements drive the expression of the marker gene in major parts of the peripheral nervous system, as well as in more restricted parts of the central nervous system. These structures can be visualized during embryonic development, allowing detailed neuroanatomical studies in midgestation embryos. We describe the β-galactosidase expression in wild-type L17 mice and demonstrate the applicability of L17 mice to the study of the nervous system. We then apply this experimental system to the analysis of *Splotch* embryos. Our findings underline the importance of *Pax3* in the development of neural crest-derived structures, especially of cranial ganglia and nerves. We suggest the use of L17 mice as a valuable tool to perform similar analysis for other embryonal mutant phenotypes.

INTRODUCTION

The *Splotch* (*Sp*) mutant is a well-recognized model for neural crest and neural tube defects (Auerbach, 1954). In the heterozygous state, it causes mild pigmentation deficiencies (white spotting). In the homozygous state, these mutants are midgestation lethals presenting phenotypic defects associated with the brain (exencephaly), the neural tube (spina bifida), muscles (absence of limb muscles), and various neural crest derivatives (e.g., dorsal root ganglia, melanocytes, thyroid, parathyroid, thymus, Schwann cells; Auerbach, 1954; Bober *et al.*, 1994; Franz, 1989, 1990, 1993; Grim *et al.*, 1992; Moase and Trasler, 1989, 1990; Yang and Trasler, 1991).

[1] To whom correspondence should be addressed. Fax: 049 551 201 504.

The murine *Pax3* gene belongs to the paired-box-containing multigene family (Goulding *et al.*, 1991; Walther *et al.*, 1991). As a member of this transcription factor family, it harbors the well-conserved paired domain of 128 amino acids which mediates the specificity and affinity of the DNA recognition process (Chalepakis *et al.*, 1994; Czerny *et al.*, 1993). In addition, *Pax3* also contains a paired-type homeodomain of 60 amino acids synergistically acting with the paired domain in the binding process. Various alterations within the *Pax3* gene appear to underlie the phenotypic defects associated with the *Sp* developmental mutant. All *Sp* alleles characterized molecularly have revealed the presence of mutations within the *Pax3* gene: *Sp*, Sp^{d}, Sp^{r}, Sp^{1H}, Sp^{2H}, and Sp^{4H} (Epstein *et al.*, 1991a,b, 1993; Goulding *et al.*, 1993; Vogan *et al.*, 1993).

The molecular basis of a human developmental syndrome has also been demonstrated to depend on mutations affect-

0012-1606/95 $12.00

ing the human *PAX3* gene. The Waardenburg's syndromes, which constitute a genetically heterogeneous family of dominant disorders, present phenotypic features associated with cranial neural crest deficiencies. Typically, affected individuals present craniofacial abnormalities including dystopia canthorum (increased distance between the inner corners of the eyes), prominent nasal root, cleft-lip and highly arched palate, various pigmentation deficiencies (comprising heterochromia irides, white forelock and eyelashes, premature greying, hypopigmented skin patches), and sensorineural deafness (McKusick, 1992; Waardenburg, 1951). Other infrequent phenotypic features that have been reported include spina bifida and meningomyelocele (Arnvig, 1959; Chatkupt *et al.*, 1993; Pantke and Cohen, 1971). Diverse alterations within the *PAX3* gene have now been genetically linked to the appearance of some of these syndromes as alterations affecting well-conserved residues of the paired box or resulting in premature translation termination at various positions within the PAX3 protein have been documented in Waardenburg's patients (Baldwin *et al.*, 1992; Butt *et al.*, 1994; Foy *et al.*, 1990; Hoth *et al.*, 1993; Ishikiriyama *et al.*, 1989; Tassabehji *et al.*, 1992, 1993).

Although the phenotypic similarities between *Sp* and Waardenburg mutations are striking in many aspects (neuroectoderm-, limb muscle-, and trunk neural crest-associated deficiencies), other aspects of the phenotype have not been matched between the human condition and the murine model. For instance, although prominent craniofacial defects, presumably of neural crest origin, are readily observed in the Waardenburg's syndrome (heterozygous state), no cranial neural deficiencies have been yet documented for the *Sp* mutant. Since the most prominent and best described neural crest deficiency at the trunk level in the *Sp* mutant lies in the dorsal root ganglia dysgenesis, we have followed the development of cranial ganglia and nerves in normal as well as in *Sp* and Sp^d homozygous embryos. In order to facilitate the study and gain a better insight into the three-dimensional organization of cranial ganglia and nerves, the development of these structures was monitored using the L17 transgenic mouse line. L17 constitutes a unique transgenic mouse line originally generated in the context of an investigation of the Hoxa-7 promoter in transgenic mice (Püschel *et al.*, 1991). In L17 mice, expression of the Hoxa-7/lacZ construct (pm6lacZ11) is not only dependent on the promoter fragment, but also on the genomic site of integration. In combination, the two parameters result in a lacZ expression pattern confined almost exclusively to the nervous system, mostly of the peripheral, but also including specific regions of the central nervous system (Kessel, 1993; Püschel *et al.*, 1991). Before Day 10.0 the lacZ expression was confined to the normal Hoxa-7 expression domain. It was observed in the ventral neural tube, the dorsal root ganglia, and the dermomyotome, respecting the anterior boundaries typical for Hoxa-7 (C4–C5 for the neural tube and dorsal root ganglia, and T3–T2 for the mesoderm; Püschel *et al.*, 1991), and thus no staining was visible in the head. In this communication, we first report the development of the wild-type pattern observed in L17 mice. We then used the L17 transgene to analyze the nervous system of *Splotch* mice, which lack a functional *Pax3* gene. The development of dorsal root ganglia development has been reexamined in the *Sp* and Sp^d mutants. In addition, our results indicate that *Pax3* is essential for the proper development of cranial ganglia to which neural crest cells have been shown to contribute. The *Pax3* deficiency affects both their formation and their ability to send out peripheral projections. Finally, this study underlines the interest of using the L17 transgenic mouse line in order to follow for different purposes the development of trunk and cranial ganglia as well as peripheral nerves.

RESULTS

Neuroanatomy of Wild-Type L17 Mice

Our study concentrated on the period between Days 10.5 and 13.5 p.c., which is most critical to follow formation of peripheral ganglia and nerves. The integrity of whole-mount-stained embryos allowed us to analyze the labeled structures further by a variety of techniques. This included extensive manual dissection, gelatine/albumin embedding followed by vibratome sectioning (30–100 μm), standard histology using paraffin sections (8–10 μm), or retrograde labeling of nuclei using lipophilic dyes (e.g., dioctadecyl-tetramethyl-indocarbocyanine perchlorate; DiI). Since lacZ expression appears not to be affected by the genetic background (NMRI and C57Bl/6), the L17 line was bred with existing mutants in order to evaluate their neuroanatomy. The typical staining pattern of L17 embryos at Day 12.5 p.c. is presented in Fig. 1 and the results obtained are tabulated for different developmental stages up to Day 13.5 p.c. (Table 1). In the head, the most strikingly marked structures are the cranial nerves, the cranial ganglia, and their motor nuclei. The oculomotor (III), the trochlear (IV), the trigeminal (V), the facial (VII), the glossopharyngeal (IX), the vagal (X), and the accessory (XI) cranial nerves were clearly labeled. In particular, the progression and arborization at the head level could be followed (e.g., the branches of nerve V: ophthalmic, frontal, maxillary, and mandibular nerves). Strong staining of cranial ganglia was observed in particular in the trigeminal (V), geniculate (VII), superior (IX), and jugular (X) ganglia, as well as in numerous small transitory hindbrain ganglia including Froriep's ganglion (Figs. 1 and 2). On the other hand, only a weak labeling of the hypoglossal nerve (XII) was visible. Only a few cells of the vestibulocochlear ganglion (VIII) expressed the transgene. Also within the central nervous system several regions of strong staining were detected (Fig. 1) and identified after vibratome sectioning. These included the telencephalic septum, the hypothalamus, and the ventral thalamus (Fig. 1 and data not shown). The origin of the motor axons, namely the motor nuclei of nerves III and IV in the floor of the mesencephalon, of nerve V in the floor of rhombomeres 2 and 3 (R2 and R3),

TABLE 1
Developmental Expression of the L17 Transgenic β-Galactosidase Marker Gene

Structures	Age (days p.c.)				
	9.5	10.5	11.5	12.5	13.5
Telencephalic septum	−	−	+	+	+
Thalamus	−	−	+	+	+
Motor nucleus (III/IV)	−	+	+	+	+
Nerve (III/IV)	−	+	+	+	+
Mesencephalic sensory nucleus (V)	−	+	+	+	+
Trigeminal ganglion (V)	−	+	+	+	+
Ophthalmic nerve (V)	−	±	+	+	+
Maxillary nerve (V)	−	+	+	+	+
Mandibular nerve (V)	−	±	+	+	+
Motor nucleus (V)	−	±	+	+	+
Spinal sensory nucleus (V)	−	±	+	+	+
Facial nerve (VII)	−	±	+	+	+
Motor nucleus (VII)	−	+	+	+	±
Superior ganglion (IX)	−	−	+	+	+
Jugular ganglion (X)	−	−	+	+	+
Accessory nerve (XI)	−	−	+	+	±
Neural tube	−	+	+	+	+
Dorsal root ganglion	±	+	+	+	+

and of nerve VII in R4 and R5 were labeled within the basal plate (Figs. 1 and 2). In the alar plate, the mesencephalic sensory and spinal sensory nuclei of the trigeminal were visible. Notably, structures and nuclei associated with the olfactory nerve (I), optic nerve (II), and abducens nerve (VI) were not stained in the L17 line.

Developmental Expression of the L17 β-Galactosidase Marker

In order to obtain a precise description of the development of ganglia and nerves stained in the L17 transgenic mouse, stained embryos were dissected and analyzed in detail between Days 10.5 and 13.5 p.c. (Fig. 2). At Day 10.5 (n = 4; Figs. 2A and 2D), the III, IV, V, and VII motor nuclei started to be visible. The oculomotor, trochlear, and facial nerves as well as the various branches of the trigeminal started to emerge (Figs. 2A and 2D). Newly stained structures appeared at Day 11.5 p.c. (n = 15; Figs. 2B and 2E). At that stage, the frontal nerve emerging from the ophthalmic lobe of the trigeminal ganglion had already reached the ventrolateral side adjacent to the telencephalon and the maxillary branch had met with the most distal part of the maxillary process and was producing multiple arborizations, while the mandibular branch had progressed well into the first arch forming the mandibule. On the other hand, the medially located motor nuclei of the trigeminal (R2) were less evident than at Day 10.5 p.c. (Figs. 2B and 2E). At that stage, at the pons level, a strong staining appeared in the trigeminal sensory nucleus while the trigeminal sensory spinal fibers as well as the R5-located motor nuclei of the facial nerve started to stain within the hindbrain (Figs. 2B and 2E). At the level of the third arch, cells expressing β-galactosidase started to organize in the proximal (superior) ganglia of the IX and X nerves (Figs. 2C and 2F). Slightly more caudal, groups of cells organized into small ganglia and joined by axonal bundles started to appear on Day 11.5, but were rarely detected (4% of the cases) on Day 13.5, probably reflecting the transitory nature of these ganglia. The faint staining observed on the accessory nerve as it passes longitudinally on Days 11.5 and 12.5 (Fig. 4) was sometimes detected (32%) on Day 13.5.

The labeled structures appeared clearest at Day 12.5 p.c. (n = 25; Figs. 1A, 2C, and 2F). At this stage, staining within the brain could clearly be discerned in the septum, the hypothalamus, and the ventral thalamus (Fig. 2F). The III and IV cranial nerves had reached their target in the eye region (Fig. 2F) while the trigeminal frontal nerve had reached the frontonasal region and was producing lateral branches. The development of the maxillary, mandibular, and masticatory branches, the spinal sensory tracts of the trigeminal ganglion, the facial nerve, and the superior (IX)/jugular (X) complex had also further progressed at this stage. However, projections of the superior and jugular ganglia toward the sympathetic trunk failed to stain while branches extending anteriorly, probably corresponding to auricular, tympanic, hyoid, and/or glossal branches, were visible (Fig. 1B). Dorsal projections running from the superior/jugular complex were more numerous and the small caudally located ganglia had also further developed. Motor nuclei of the III, IV, V, and VII were still strongly stained at that stage (Figs. 2D and 2H).

In order to verify whether the labeling of motor neuron pools includes all motor neurons or only a subset, retrograde labeling of the facial nerve was performed using DiI and compared with β-galactosidase staining at Day 11.5 p.c. embryo (Fig. 3; Godement *et al.*, 1987). Staining of the L17 embryos labelled medially located motor neurons at the

FIG. 1. β-Galactosidase staining of a Day 12.5 p.c. embryo from the L17 transgenic mouse line. Lateral view. Only one half of the embryo is depicted; a glycerol-cleared embryo was bisected by making a sagittal incision from the ventral part of the embryonic face up to the neural tube and the floor of the mesencephalon. lacZ-positive structures are identified by numbers.

FIG. 2. Developmental expression pattern of the β-galactosidase marker at the cranial level in the L17 transgenic mouse line. Lateral views are presented at Days (A) 10.5, (B) 11.5, and (C) 12.5 p.c. with the corresponding ventral views (D, E, and F). Numbers indicate structures as designated in Fig. 1.

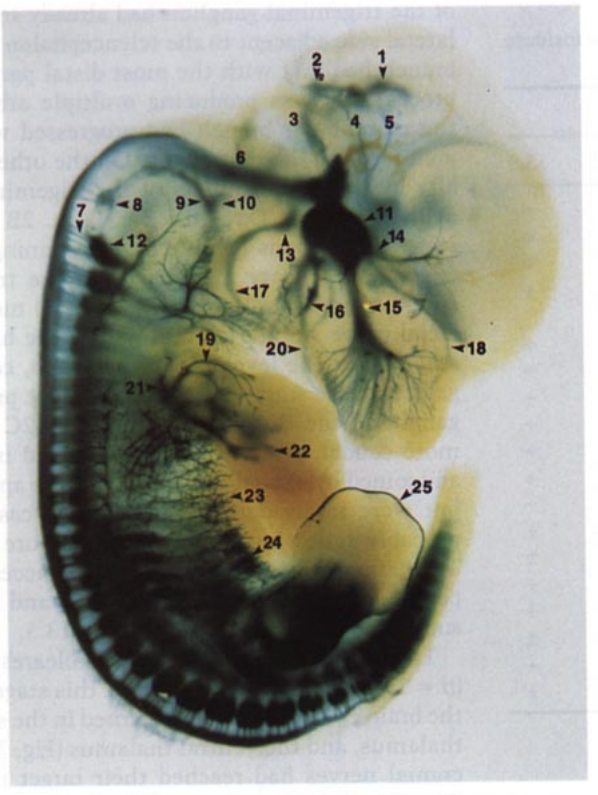

1

1 Motor nucleus (III)
2 Motor nucleus (IV)
3 Mesencephalic sensory nucleus
4 Trochlear nerve (IV)
5 Oculomotor nerve (III)
6 Spinal sensory nucleus (V)
7 Dorsal roots
8 Froriep's ganglion
9 Jugular ganglion (X)
10 Superior ganglion (IX)
11 Trigeminal ganglion (V)
12 Dorsal root ganglion
13 Geniculate ganglion (VII)
14 Ophthalmic nerve (V)
15 Maxillary nerve (V)
16 Masticatory nerve (V)
17 Facial nerve (VII)
18 Frontal nerve (V)
19 Radial nerve (
20 Mandibular nerve (V)
21 Brachial nerve
22 Digital nerves
23 Intercostal nerves
24 Dermomyotome
25 Apical ectodermal ridge
26 Motor nucleus (VII)
27 Septum
28 Ventral thalamus
29 Hypothalamus
30 Accessory nerve (XI)
31 Motor nucleus (V)

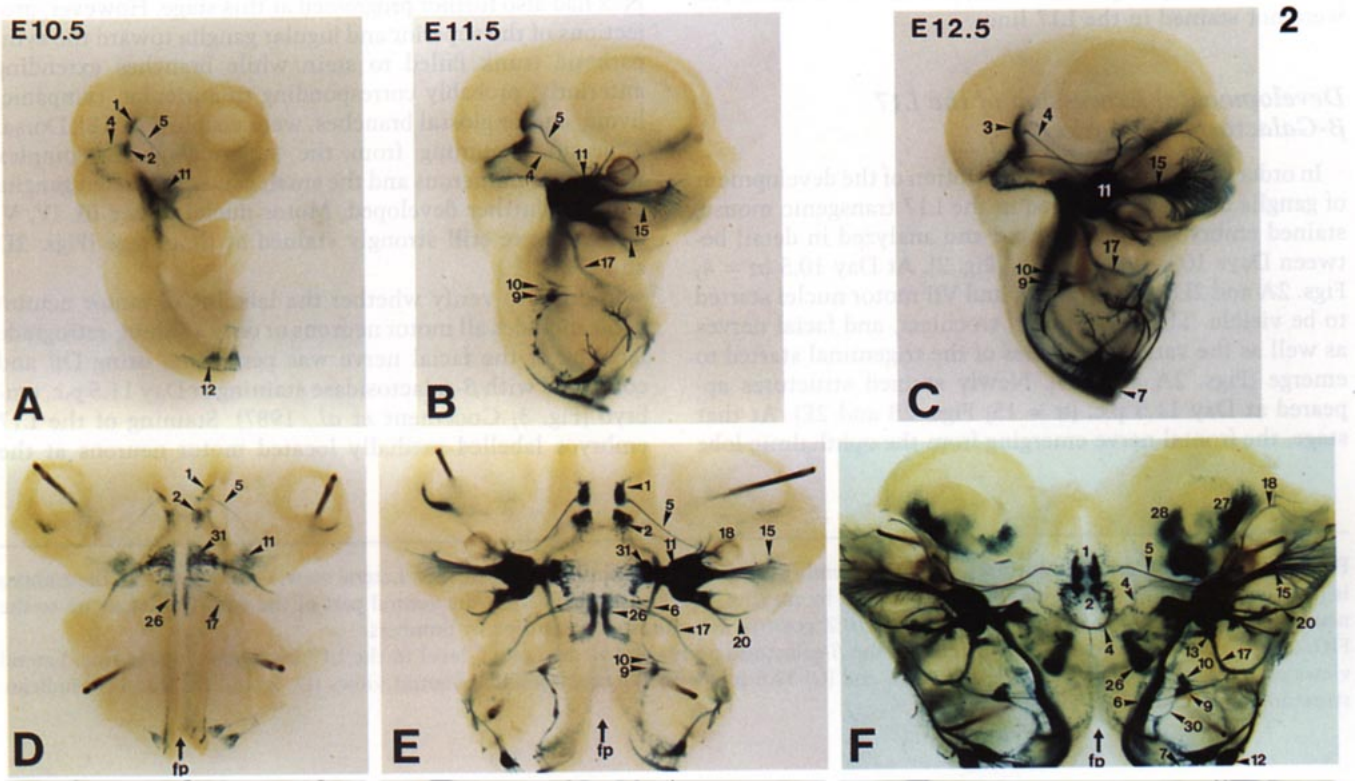

2

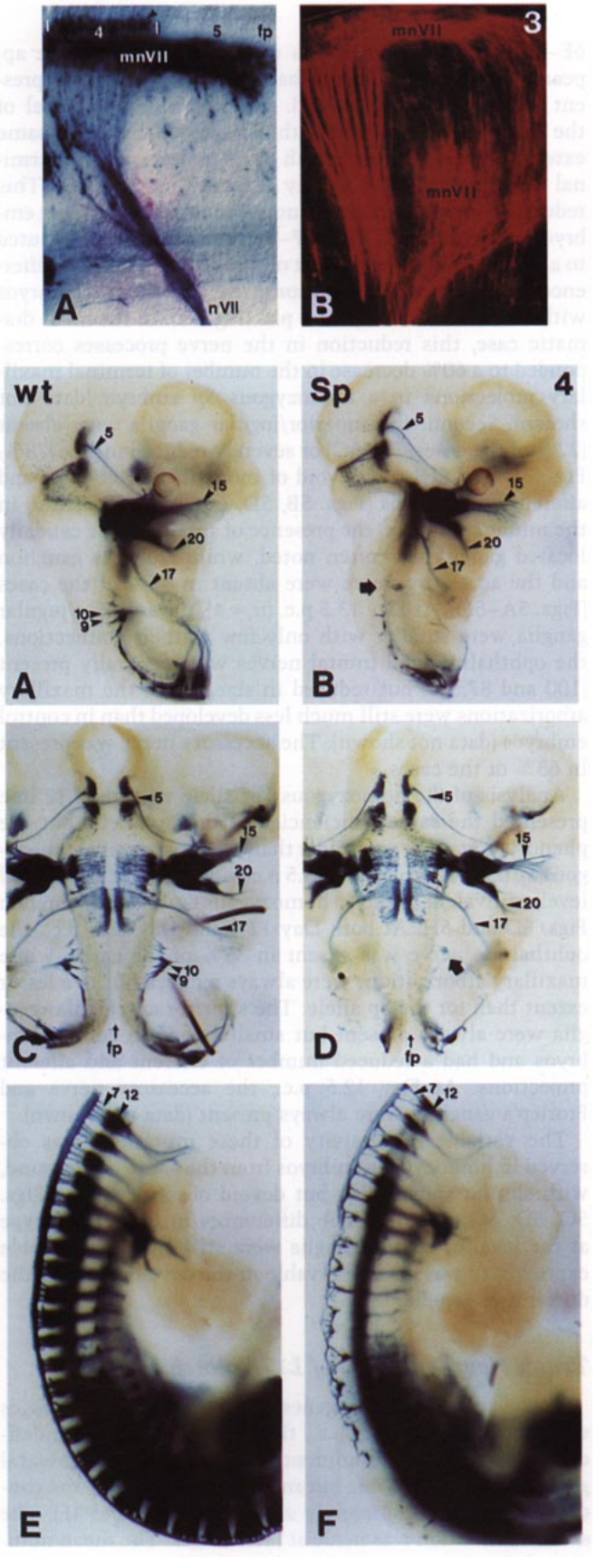

floor of R4 and R5 with their axons exiting through R4. In addition, contralaterally migrating motor neurons (R4 level) such as those recently described in the chick were also weakly labeled (Simon and Lumsden, 1993). In contrast, DiI labeling visualized the same pools as well as a laterally located pool with axons running laterally to join the facial nerve exiting at the R4 level. This laterally located R5 nucleus detected with DiI has not been documented in the chick (Lumsden and Keynes, 1989). It is not clear if it represents indeed a portion of the facial motor nucleus or if we labeled sensory fibers of the intermediate nerve, which joins the facial nerve to exit together from the brain. These data indicate that the β-galactosidase labeling of the L17 line detected at least a major portion of the motor neuron pool contributing to the facial nerve.

The Peripheral Nervous System at the Trunk Level of Wild-Type L17 Mice

At the trunk level, dorsal root ganglia and peripheral nerve development could also be followed. Peripheral nerves contain sensory components from the spinal ganglia and motoric components and autonomic components from the sympathetic trunk. Dorsal afferent ascending fibers have their cell bodies within the dorsal root ganglia, presumably corresponding to the fibers forming the gracile and cuneate fascicles later on (Figs. 1 and 7). Small clusters of scattered label were also observed dorsally, possibly corresponding to sensory axons projecting from the dorsal root ganglia. The sympathetic trunk also presented some staining while the development of the nerves could be followed as the sensory components from the spinal ganglia as well

FIG. 3. Visualization of the facial motor nuclei at Day 11.5 p.c. (A) β-Galactosidase staining of the facial motor nucleus (mnVII) at the level of rhombomere 4 (4) and rhombomere 5 (5) in a L17 transgenic embryo. Cell bodies are located alongside the floorplate (fp). Cells transgressing into the floorplate are restricted to R4 (arrowhead). The facial nerve (nVII) exits from the alar plate at the level of rhombomere 4. (B) Staining of the facial motor nuclei (mnVII) as observed by retrograde labeling using DiI. An additional group of cell bodies, not visible by β-galactosidase staining, is visualized, which also exits together with the facial nerve.

FIG. 4. Comparison of the L17 β-galactosidase-expressing structures at Day 11.5 p.c. in normal (A, C, and E) and homozygous *Sp* embryos (B, D, and F). (A and B) Lateral view at the cranial level. Development of the superior (IX, No. 10) and jugular (X, No. 9) ganglia is deficient in homozygous *Sp* embryos (broad arrow). (C and D) Ventral view at the cranial level. The ganglionic deficiency is asymmetrical. While a small ganglion is observable on the right side (broad arrow) of the *Sp* homozygous embryo, no ganglion is observable on the left side. The position of the floorplate (fp) is indicated by a small arrow. (E and F) Lateral view at the trunk level. Only a few small dorsal root ganglia and severely deficient dorsal roots are observed in the mutant at cervical and upper thoracic levels. Numbers indicate structures as designated in Fig. 1.

as motor nerves emerging from the ventral horns extended into the periphery (Fig. 7A). As could be detected from various sections at Day 12.5 p.c., all of the rami of the spinal nerves have been identified by β-galactosidase staining; dorsal ramus, ventral ramus, intercostal ramus (Fig. 7A), anterior ramus, and ramus communicans were all strongly labeled. In the neural tube, the labeled domains encompassed the floor plate as well as the ventral motor neuron columns (Fig. 7).

Cranial Neuroanatomy of L17/Splotch Mice

In order to determine whether the development of cranial ganglia and nerves is affected in *Sp* animals, the L17 transgenic line was crossed with *Sp* and Sp^d alleles and homozygous embryos harboring the β-galactosidase transgene were obtained. The phenotypic features observed are presented in Figs. 4, 5, 6, and 7.

Homozygous *Sp* and Sp^d animals were recognizable starting around Day 10.0 p.c. by the presence of lumbosacral spina bifida of various severity sometimes accompanied by exencephaly (*Sp*, 50%; Sp^d, 20%). Homozygosity was generally confirmed by the presence of dorsal root ganglion dysgenesis in these embryos (Figs. 4 and 6). All of the embryos presenting dorsal root ganglia dysgenesis were affected by spina bifida, while one Sp^d embryo presenting only very mild spina bifida in the tail region displayed normal development of spinal ganglia. Neither the importance of the spina bifida nor the presence of exencephaly appeared to influence other phenotypic parameters. Phenotypic changes observed in various structures were variable in agreement with previous reports describing the variable expressivity of *Sp* mutations (Auerbach, 1954; Yang and Trasler, 1991).

While all motor nuclei at the level of the mesencephalon and hindbrain (III, IV, V, VII) remained normal in homozygous embryos, the development of some cranial ganglia and nerves was strongly affected by both the *Sp* and the Sp^d mutations. Prominent changes were associated with the development of the trigeminal system, with the superior ganglia of the 9th and 10th cranial nerves and, to a lesser extent, with Froriep's ganglion and the accessory nerve.

Homozygous *Sp* embryos presented clear phenotypic manifestations in jugular ganglion starting at Day 11.5 p.c. ($n = 5$; Fig. 4). At that stage, the normal staining of the superior/jugular ganglia revealed efferent and afferent processes (Figs. 4A and 4C). In homozygous *Sp* embryos, these ganglia were either very small (80% of the cases) or completely absent (20%; Figs. 4B and 4D). In addition, their efferent and afferent projections were generally completely missing (80%) at that stage.

At Day 12.5 p.c., homozygous *Sp* embryos analyzed presented a clearer picture of the phenotypic changes ($n = 12$; Figs. 5 and 6). First, changes were observed in the trigeminal system. While the structure of the ganglion appeared normal, some nerves projecting from it were affected. The frontal nerve, emerging from the ophthalmic branch of this ganglion, was most of the time absent at that stage (71%; Figs. 6E–6H). When present (29% of the cases), this nerve appeared undersized. The ophthalmic nerve was always present but was also undersized. In addition, at the level of the maxillary component, although developed to the same extent in respect to the length of its projections, the terminal arborizations were greatly reduced (Figs. 6E–6H). This reduction was extremely pronounced when comparing embryos of Day 12.5 p.c. (Figs. 6F–6H) and cannot be attributed to a delay in the development of this structure as this difference was also evident when comparing the mutant embryos with controls from Day 12.0 p.c. (Fig. 6E). In the most dramatic case, this reduction in the nerve processes corresponded to a 60% decrease in the number of terminal maxillary projections in a homozygous *Sp* embryo (data not shown). Second, the superior/jugular ganglia were absent (22% of the cases; Fig. 6G) or severely reduced in size (78%; Figs. 5D and 6H) and devoid of most of their efferent and afferent connections (Figs. 5B, 5D, 6G, and 6H). Third, in the mutant embryos, the presence of small ectopic caudally located ganglia was often noted, while Froriep's ganglion and the accessory nerve were absent in 46% of the cases (Figs. 5A–5D). At Day 13.5 p.c. ($n = 4$), the superior/jugular ganglia were smaller with only few of their connections, the ophthalmic and frontal nerves were generally present (100 and 87.5%) but reduced in size, while the maxillary arborizations were still much less developed than in control embryos (data not shown). The accessory nerve was present in 63% of the cases.

Analysis of the homozygous Sp^d allele with the L17 line presented the same deficiencies as the *Sp* allele, but the phenotype was always milder than the most severe homozygous *Sp* (Day 12.5 p.c., $n = 13.5$ p.c., $n = 4$) and, at the cranial level, equivalent to the *Sp* homozygous embryo presented in Figs. 6D and 6H. At both Day 12.5 and Day 13.5 p.c., the ophthalmic nerve was absent in 33% of the cases, while maxillary arborizations were always reduced but to a lesser extent than for the *Sp* allele. The superior and jugular ganglia were always present but smaller than in control embryos and had a reduced number of efferent and afferent projections. At Day 12.5 p.c., the accessory nerve and Froriep's ganglion were always present (data not shown).

The variable expressivity of these mutations was observed in homozygous embryos from the same background, with similar spina bifida but devoid of exencephaly (Figs. 5C, 5D, 5G, and 5H). The differences in their phenotype at the level of cranial ganglia were striking. This variable expressivity was also observable in the development of the dorsal root ganglia.

Trunk Neuroanatomy of L17/Splotch Mice

Dorsal root ganglia dysgenesis was observed at all stages examined. At Day 11.5 p.c., the dorsal root ganglion deficiency was already prominent. Although the most rostral ganglia were still visible but much smaller in size, the caudal ganglia were completely absent (Figs. 4E and 4F). The same observation was made at later stages. The mean num-

ber of spinal ganglia observed for the homozygous *Sp* embryos was 9.1 ($n = 21$, $\pm$ 2.6). Dysgenesis of the dorsal root ganglia was less pronounced in Sp^d embryos as they presented a mean of 21.4 ganglia ($n = 7$, $\pm$ 2.7). In no instance were less than 18 ganglia observable in Sp^d embryos.

As seen by vibratome sectioning, at midthoracic level these homozygous *Sp* embryos ($n = 4$; Day 12.5 p.c.) presented staining at the level of the floor plate and motor neuron columns (Fig. 7B). However, while the floor plate signal was always stronger, the motor neuron staining was still organized in columns and sending out axons ventrally. On the other hand, the sympathetic ganglia were always of a much smaller size. Interestingly, at lower lumbar level, where spina bifida was observed, the floor plate signal was extremely intense while the motor neuron signal was disorganized and scattered over the medial part of the flat neuroepithelium, corresponding to what would have formed the ventral spinal cord in a properly shaped neural tube (Fig. 7D).

Cranial Expression of the Pax3 Gene

Starting at Day 9.5 p.c. the *Pax3* gene is expressed in the dorsal part of the neural tube, hindbrain, and mesencephalon. Whole-mount *in situ* hybridization at Day 11.5 p.c. is presented (Fig. 8). In addition, *Pax3* transcripts are detected in the trigeminal ganglion between Days 10 and 12 p.c. From Day 10.5 p.c., expression is also strong in the developing face and in the distal part of the hyoid and mandibular processes (Fig. 8).

DISCUSSION

Our communication describes the lacZ staining observed in L17 transgenic embryos between Days 9.5 and 13.5 p.c. As this line provides an anatomical marker for various motor and sensory nuclei as well as peripheral ganglia and nerves, it constitutes a remarkable tool to follow the development of particular components of the nervous system. At the mesencephalic level, starting at Day 10 p.c. the III and IV motor groups and their corresponding nerves (oculomotor and trochlear nerves) can be followed as they elongate toward the eye region. Adjacent to rhombomere 2, the formation of the trigeminal ganglion (V) together with its ophthalmic, maxillary, and mandibular branches were apparent, while the course of the VII nerve and its geniculate ganglion can be visualized. Staining was also localized in the proximal ganglia of the IX and X nerves, the superior and jugular ganglia, and some afferent and efferent projections, the latter probably corresponding to the auricular and tympanic branches. At the level of the hindbrain, some motoric groups present strong staining (V, VII). In addition, the L17 transgenic line presents expression within the forebrain where the β-galactosidase is detected in the septum, the hypothalamus, and the ventral thalamus. The L17 lacZ can be utilized as a neuroanatomical marker to monitor the development of ganglia and nerves in normal, transgenic, or mutant mice. This β-galactosidase marker offers the advantage of easily performed whole-mount staining and is particularly suitable for stages between Day 10 and 13 p.c. of development, stages at which whole mounts are easily performed and analyzed while the structure of cranial ganglia and nerves is being laid down. In addition, the limited number of stained cranial ganglia and nerves provides more clarity to the staining, quality difficult to obtain by the more cumbersome whole-mount immunocytochemistry (Kuratani, 1990; Kuratani and Tanaka, 1990).

The murine *Sp* mutant constitutes a well-recognized neural crest and neural tube defect model (for a review see Moase and Trasler, 1992). The multiple deficiencies documented over the years (involving the dorsal root ganglia, Schwann cells, the thymus, thyroid, parathyroid, and the truncus arteriosus) all strongly indicate that homozygous *Sp* embryos suffer from a strong neural crest deficiency at the trunk level (Auerbach, 1954; Bober *et al.*, 1994; Franz, 1989, 1990, 1993; Grim *et al.*, 1992; Moase and Trasler, 1989, 1990; Yang and Trasler, 1991). This phenotype has been shown to be caused by various alterations within the *Pax3* gene (Epstein *et al.*, 1991a,b, 1993; Goulding *et al.*,

FIG. 5. Comparison of the L17 β-galactosidase-expressing structure at Day 12.5 p.c. in normal (A and C) and homozygous *Sp* embryos (B and D) at the cranial level. (A and B) Lateral view. Froriep's ganglion (No. 8) as well a the accessory nerve (No. 30) are missing in the homozygous *Sp* embryo. Development of the superior (IX) and jugular ganglia (Nos. 9 and 10) is impaired and connections are missing in *Sp* embryos (small arrow). Small ectopic ganglia with few projections are observed (small arrows). (C and D) Ventral view. The frontal nerve (No. 18) observed in the normal embryo is absent (small arrowhead) in the mutant embryo. Asymmetry of the deficiency is seen in the small ectopically developing ganglia (small arrows) and development of the accessory nerve. The position of the floorplate (fp) is indicated. Numbers indicate structures as designated in Fig. 1.

FIG. 6. Comparison of the L17 β-galactosidase staining in Day 12.5 p.c. control and homozygous *Sp* embryos. (A and B) Control embryos at Days 12.0 and 12.5 p.c., respectively. (C and D) Homozygous *Sp* embryos at Day 12.5 p.c. (E, F, G, and H) Corresponding enlargement of the head. Defects of neural crest derivatives in *Sp* embryos are visible in the dorsal root ganglia (Nos. 7 and 12) and the superior ganglia (Nos. 10 and 9) of the glossopharyngeal and the vagal nerves (broad arrows). The development of the trigeminal nerve (No. 15), in particular its maxillary projections and its ophthalmic (No. 14) and frontonasal branches (No. 18), is impaired in homozygous *Sp* embryos. The frontonasal nerve is completely missing (arrow) while the ophthalmic is present but undersized (broad arrowhead). The arborizations of the maxillary nerve are developed to the same extent in length but are greatly reduced in number. Numbers indicate structures as designated in Fig. 1.

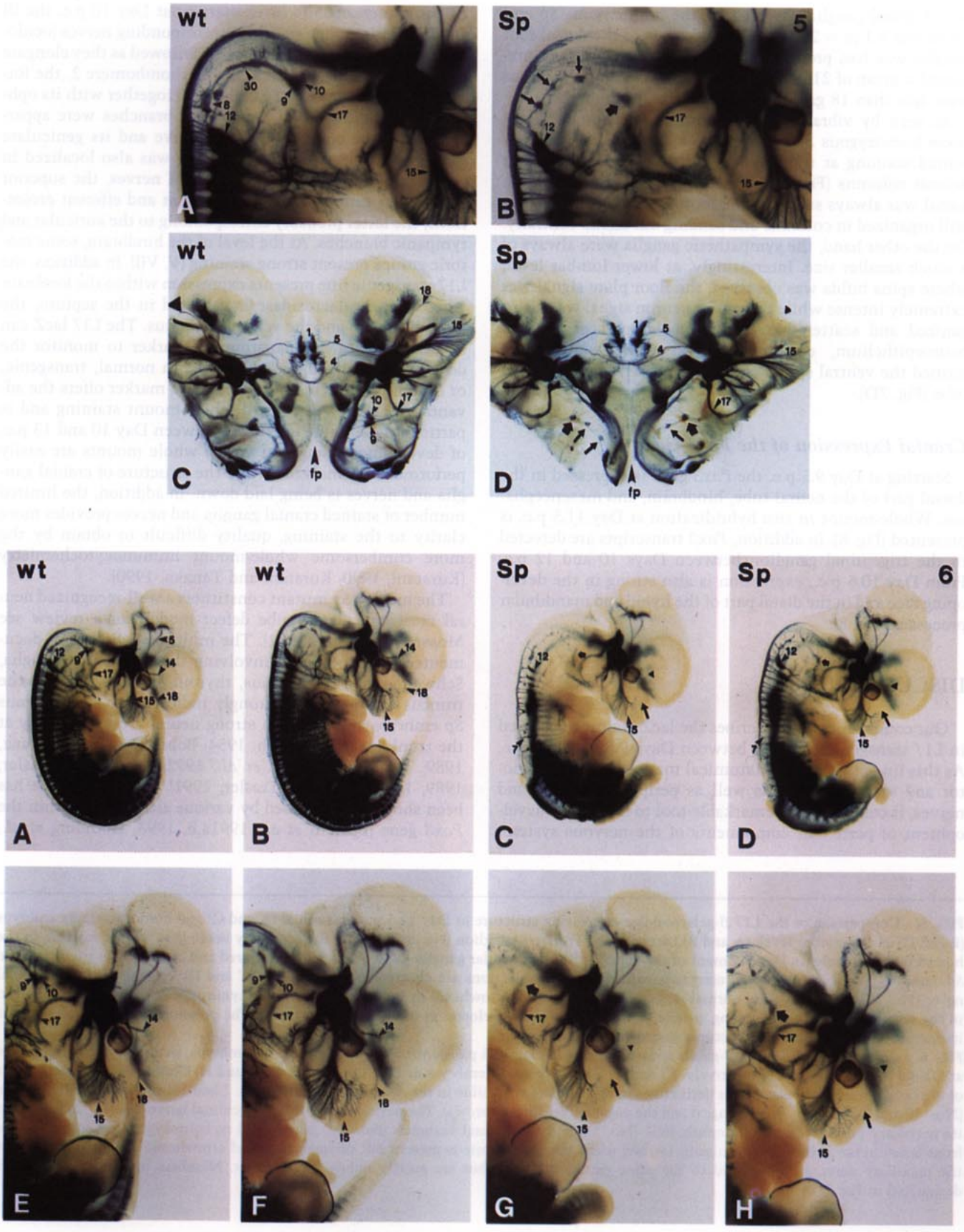

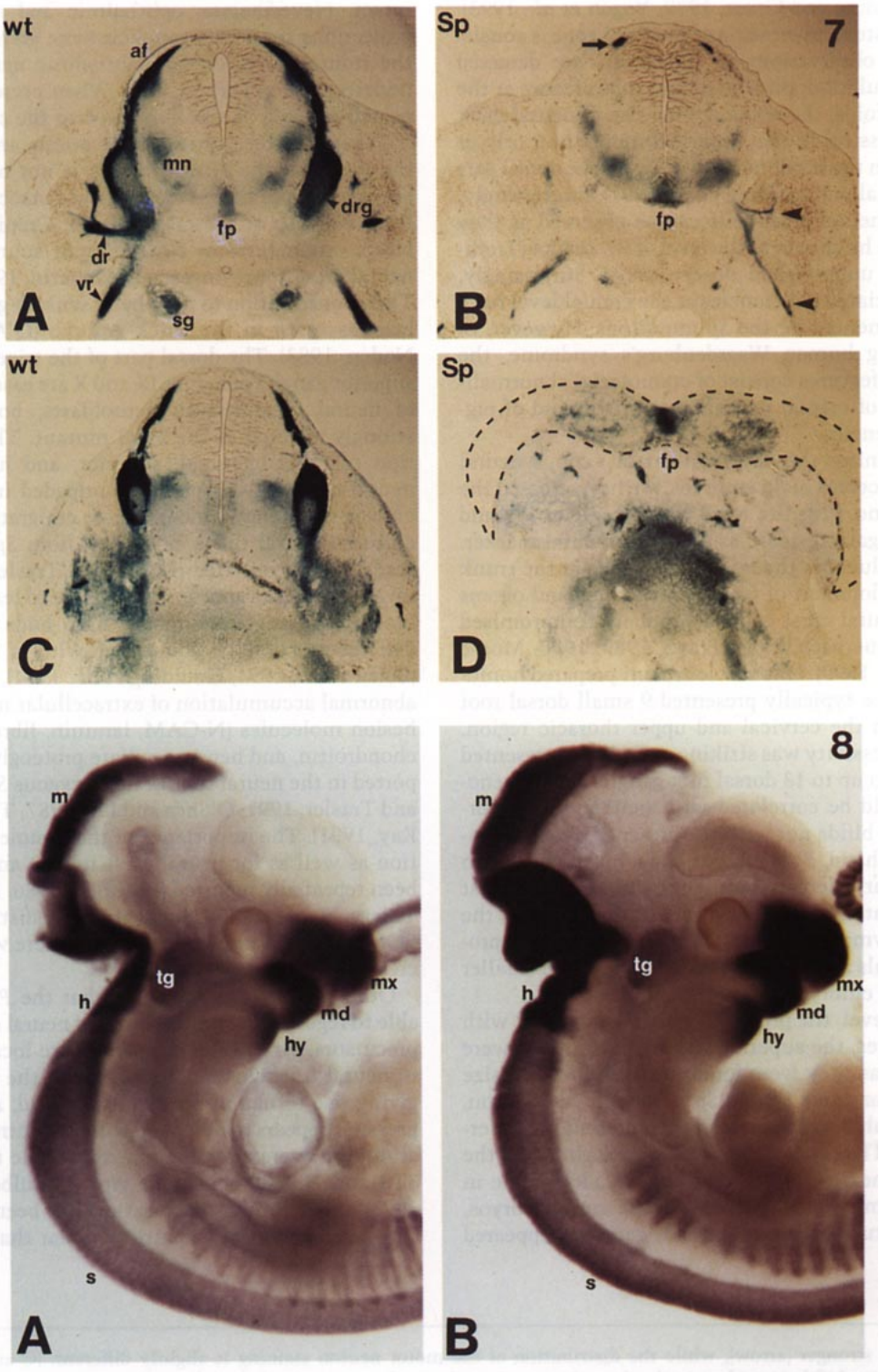

FIG. 7. Comparison of the L17 β-galactosidase staining at the trunk level as seen on vibratome sections of normal and homozygous *Sp* embryos at Day 12.5 p.c. (A and C) Normal embryo. (B and D) Homozygous *Sp* embryo. (A and B) Mid thoracic level. (C and D) Lower lumbar level. (A) In normal embryos staining can be observed in the dorsal root ganglia (drg) and peripheral nerves. The ramus dorsalis (dr) and ramus ventralis (vr), sympathetic ganglia (sg), the dorsal afferent fibers (af), motor neurons (mn), and floor plate (fp) are labeled. (B) Homozygous *Sp* animals lack dorsal root ganglia at this level and present a reduced number of dorsal afferent fibers (small arrow). Peripheral rami (arrowheads) originating from the ventral horns are still present as well as the motor neuron and floor plate signals. The

1991, 1993; Goulding and Gruss, 1989; Vogan *et al.*, 1993). In the nervous system, expression of the *Pax3* gene is consistent with these observations as transcripts are detected early during neurulation, prior to neural tube closure at the tip of the neural folds, the region giving rise to neural crest cells. *Pax3* expression is also observed more anteriorly at the cranial level in the hindbrain as well as in the dorsal part of the mesencephalon (Goulding *et al.*, 1991). Interestingly, *Pax3*-expressing neural crest cells can be observed as they migrate out of the hindbrain at the level of R2 and R4 (Tremblay and Gruss, unpublished observations). Surprisingly, neural crest-associated deficiencies at the cranial level have never been documented for the *Sp* mutations. However, in the corresponding human Waardenburg's syndrome, the main phenotypic features consist of craniofacial abnormalities, presumably of cranial neural crest origin, and of pigmentation deficiencies.

In order to monitor the development of various neural crest-derived structures of *Sp* embryos, we have crossed the L17 transgenic line with the *Pax3* mutant alleles (*Sp* and Sp^d) to use the β-galactosidase as a developmental marker. *Pax3* function influences the fate of crest cells at the trunk level, as the development of various structures and organs which require neural crest cells is seriously compromised in *Sp* embryos (Auerbach, 1954; Franz, 1989, 1990; Moase and Trasler, 1989, 1990). Our whole-mount prepared homozygous *Sp* embryos typically presented 9 small dorsal root ganglia located in the cervical and upper thoracic region. The variable expressivity was striking as embryos presented from as few as 5 to up to 13 dorsal root ganglia. This phenotypic feature could be correlated with neither the importance of the spina bifida nor with the presence of exencephaly. On the other hand, Sp^d embryos had a mean of 21 such small ganglia, clearly demonstrating the milder neural crest deficiency associated with the Sp^d allele. In addition, the development of sympathetic ganglia was seriously compromised in *Sp* animals as these were found to be much smaller than in wild-type embryos.

At the cranial level, the proximal ganglia associated with the IX and X nerves, the superior and jugular ganglia, were severely affected as they were found to be reduced in size or absent in homozygous *Sp* and Sp^d embryos. In addition, they appeared unable to send out proper afferent and efferent connections. The presence of Froriep's ganglion and the spinal accessory nerve (XI) was also often undetectable in homozygous *Sp* embryos. In contrast, in the same embryos, the general structure of the trigeminal ganglion appeared intact. Nevertheless, ophthalmic and maxillary efferent projections from this ganglion were greatly reduced while the frontal nerve of the ophthalmic nerve was generally undetectable at Day 12.5 p.c. When present, this nerve appeared reduced in size compared to the controls.

Taken together, these observations are consistent with the idea that the *Pax3* function is not only important for the integrity of neural crest-derived structures at the trunk level but also at the cranial level. Cranial sensory neuroblasts originate from two different sources: placodes and neural crest (for review see Le Douarin, 1986; Noden, 1993). Their contribution to peripheral sensory ganglia has already been assessed in the chick embryo (D'Amico-Martel and Noden, 1983). The dorsal part of the trigeminal (V) and the superior ganglia of nerves IX and X are essentially composed of neural crest-derived neuroblasts, both of which are strongly affected in the *Pax3* mutant. Thus, the colonization of the trigeminal, superior, and jugular ganglia by neural crest cells is probably impeded in homozygous *Sp* embryos. A delay in neural crest emigration from *in vitro*-cultured neural tubes extirpated from *Sp* embryos has already been postulated (Moase and Trasler, 1990). Interestingly, myoblasts appear to be unable to leave the dermomyotome and migrate into the limb buds of *Sp* animals, a deficiency possibly connected with a migration defect (Bober *et al.*, 1994; Goulding *et al.*, 1994). In the same vein, abnormal accumulation of extracellular matrix and cell adhesion molecules (N-CAM, laminin, fibronectin, collagen, chondroitin, and heparan sulfate proteoglycan) has been reported in the neural tube of homozygous *Sp* animals (Moase and Trasler, 1991; O'Shea and Liu, 1987; Trasler and Morris-Kay, 1991). The importance of these molecules for neurulation as well as for neural crest release and migration have been repeatedly reported (Edelman, 1986; Hatta *et al.*, 1987; Thiery *et al.*, 1985). Such aberrant distribution of these ECM and CAM molecules may interfere with proper neural crest function.

Other observations indicate that the *Pax3* gene may be able to regulate the proliferation of neural crest cells or their precursors. First, *Pax3* transcripts are localized early, prior to neural tube closure, at the tips of the neural folds later giving rise to neural crest cells. Second, aberrant *Pax3* expression appears to be linked with uncontrolled cell proliferation: the overexpression of *Pax3* is able to transform NIH 3T3 and 208 fibroblasts *in vitro* (Maulbecker and Gruss, 1993) and a *PAX3* translocation has been associated with the development of pediatric alveolar rhabdomyosarcomas

floor plate signal is stronger (arrow), while the distribution of the motor neuron staining is slightly different. (C and D) At the lower lumbar level, the spina bifida is evident in the *Sp* embryo and results in the reorganization of the motor neuron staining, while the floor plate signal is more intense than that in the control (C).

FIG. 8. Expression of the *Pax3* gene at the cranial level as observed by whole-mount in *in situ* hybridization at Day 11.5 p.c. (A) Normal embryo. (B) Homozygous *Sp* embryo. The distribution of the signal is similar in both embryos. Expression is seen in the dorsal part of the mesencephalon (m), hindbrain (h), spinal cord (s), in the trigeminal ganglion (tg), and the distal parts of the maxillary (mx), mandibular (md), and hyoid (hy) processes.

(Barr *et al.*, 1993; Galili *et al.*, 1993; Shapiro *et al.*, 1993). On the other hand, interactions between the placode and the neural crest cells is important for the proper development of the trigeminal ganglion: the removal of the trigeminal placode does not influence the ability of the neural crest cells to give rise to neuroblasts but impedes their ability to send out peripheral projections (Hamburger, 1961; Noden, 1978). Because this ganglion expresses the *Pax3* gene between Days 10 and 12 p.c., it cannot be excluded that, in addition to the neural crest, a trigeminal placodal component may be deficient. Finally, the potential of neural crest cells to properly differentiate and functionally contribute to the trigeminal ganglion might be impaired by the *Pax3* mutations and may compromise the ability of the neural crest-derived neurons for axonal sprouting.

In the homozygous state, *Sp* and Sp^d alleles impair the development of the trigeminal (V), superior (IX), and jugular (X) ganglia. The function of *Pax3* may be crucial for the neural crest migration and proliferation as well as their ability to differentiate into neurons capable of properly sending out axons. These new observations, at the cranial level, are of particular interest in view of the phenotypic features of the corresponding human Waardenburg's syndrome displayed at the cranial level, namely craniofacial abnormalities as well as sensorineural deafness (McKusick, 1992; Waardenburg, 1951).

EXPERIMENTAL PROCEDURES

Mice

Sp and Sp^d mouse lines, obtained from Jackson Laboratories (Bar Harbour), were bred with C57BL/6. The previously produced transgenic mouse line L17, which harbors a β-galactosidase marker under the control of a Hoxa-7 promoter element, was bred on an NMRI or C57Bl/6 background. Embryos were obtained from (L17/+; *Sp*/+)F1 × *Sp*/+ and (L17/+; Sp^d/+)F1 × Sp^d/+ crosses. Control L17 embryos were produced by crossing L17 (NMRI or C57Bl/6) transgenic animals with NMRI or C57BL/6 wild-type animals.

The embryonal stages were evaluated counting the morning of appearance of the vaginal plug as Day 0.5 p.c. They were dissected out at the appropriate stages, isolated from surrounding membranes, and rinsed in PBS. For histology, embryos were immediately fixed overnight at 4°C in 4% paraformaldehyde prepared in phosphate-buffered saline (PBS). On the next day, embryos were dehydrated through an ethanol/saline series, treated with xylene, and embedded in paraplast (Monoject Scientific). For β-galactosidase staining, fixation was performed for 30 min at 4°C in 1% formaldehyde/0.2% glutaraldehyde/0.2% NP40/0.1% sodium deoxycholate/PBS. The embryos were then washed twice in PBS for 20 min at 4°C. Staining was obtained by overnight incubation at 30°C in 0.1% X-Gal (dissolved in dimethylformamide) with 5 m*M* $K4F(CN)_6$, 5 m*M* $K3F(CN)_6$, 2 m*M* $MgCl_2$, 0.2% NP40, and 0.1% sodium deoxycholate. From Day 13.5 onward, staining of some structures appeared with variability, while some expression domains vanished. The progressively weakening signal encountered at later developmental stages is likely to result from the Hoxa-7 elements controlling the expression of the lacZ marker, which in their normal context drive the highest expression between Days 9.5 and 13.5 p.c. In addition, the whole-mount procedure becomes increasingly problematic in more compact embryos. Dissection prior to staining improves the penetration and allows visualization of remaining expression domains later in embryogenesis (Day 15.5 p.c. or older). After staining, embryos were either cleared in glycerol/PBT solution (30, 50, and 80%) or embedded in a mixture of gelatine/albumen/sucrose and sectioned at 50 μm using a Pelco 101 vibratome. Sections were mounted on gelatin-subbed slides and photographed with a Zeiss Axiophot microscope using bright-field illumination. Ventral views of whole mounts were obtained by making a sagittal incision from the ventral part of the embryonic face up to the neural tube and the floor of the mesencephalon and immobilizing the specimens onto a silicon surface (Sylgard dish) with insect needles. Lateral views were obtained by cutting glycerol-treated embryos sagittally into halves. Cleared embryos were photographed under a Zeiss SV11 stereomicroscope. Quantification of the number of maxillary arborizations was estimated using coronal vibratome sections of normal and homozygous embryos. The images used for this quantification were acquired using Adobe Photoshop (Adobe Systems Inc.) and a Nikon N8008S camera to facilitate the estimation of maxillary projections.

Whole-Mount in Situ Hybridization

Expression of the *Pax3* gene was analyzed by *in situ* hybridization using a 520-bp *Hin*dIII/*Pst*I fragment of the cDNA. It encodes the 3′ part of the paired-type homeodomain and most of the carboxy terminus (Goulding *et al.*, 1991). Mouse embryos were collected and treated as previously described (Bober *et al.*, 1994).

Retrograde Labeling of Cranial Nerves

The mouse embryos were dissected out of the uterus, fixed, and stained as already described. The animals were immobilized in agarose dishes and the facial nerve was dissected free distal to the geniculate ganglion. Crystals of DiI C18 (Molecular Probes; 1,1′-dioctadecyl-3,3,3′,3′-tetramethyl-indocarbocyanine perchlorate) were applied on the tip of the nerve and left in place until the dye had reached the neuronal bodies in the floor of the hindbrain (Godement *et al.*, 1987). The embryos were then extensively washed with PBS and the hindbrain was dissected out. The pictures of retrograde labeling were made using epifluorescence with Zeiss filters (09 and 15) with a Zeiss Axiophot microscope using 1600 Ektachrome film.

ACKNOWLEDGMENTS

We wish to thank C. Müller for exceptional technical assistance and T. Franz, A. Stoykova, and F. Pituello for critical reading of the manuscript. P.T. was the recipient of a fellowship from the Medical Research Council of Canada. This work was supported by the Max Planck Society.

REFERENCES

Arnvig, J. (1959). The syndrome of Waardenburg. *Acta Genet.* **9,** 41–46.

Auerbach, R. (1954). Analysis of the developmental effects of a lethal mutation in the house mouse. *J. Exp. Zool.* **127,** 305–329.

Baldwin, C. T., Hoth, C. F., Amos, J. A., da-Silva, E. O., and Milunski, A. (1992). An exonic mutation in the HuP2 paired domain gene causes Waardenburg's syndrome. *Nature* **355,** 637–638.

Barr, F. G., Galili, N., Holick, J., Biegel, J. A., Rovera, G., and Emanuel, B. S. (1993). Rearrangement of the PAX3 paired box gene in the pediatric solid tumor alveolar rhabdomyosarcoma. *Nature Genet.* **3,** 113–117.

Bober, E., Franz, T., Arnold, H.-H., Gruss, P., and Tremblay, P. (1994). *Pax3* is required for the development of limb muscles: A possible role for the migration of dermomyotomal muscle progenitor cells. *Development* **120,** 603–612.

Butt, J., Greenberg, J., Winship, I., Sellars, S., Beighton, P., and Ramesar, R. (1994). A splice junction mutation in PAX3 causes Waardenburg syndrome in a South African family. *Hum. Mol. Genet.* **3,** 197–198.

Chalepakis, G., Goulding, M., Read, A., Strachan, T., and Gruss, P. (1994). Molecular basis of *Splotch* and Waardenburg *Pax3* mutations. *Proc. Natl. Acad. Sci. USA* **91,** 3685–3689.

Chatkupt, S., Chatkupt, S., and Johnson, W. G. (1993). Waardenburg syndrome and myelomeningocele in a family. *J. Med. Genet.* **30,** 83–84.

Czerny, T., Schaffner, G., and Busslinger, M. (1993). DNA sequence recognition by Pax proteins: Bipartite structure of the paired domain and its binding site. *Genes Dev.* **7,** 2048–2061.

D'Amico-Martel, A., and Noden, D. M. (1983). Contributions of placodal and neural crest cells to avian cranial peripheral ganglia. *Am. J. Anat.* **166,** 445–468.

Edelman, G. M. (1986). Cell adhesion molecules in the regulation of animal form and tissue pattern. *Annu. Rev. Cell Biol.* **2,** 81–116.

Epstein, D. J., Malo, D., Vekemans, M., and Gros, P. (1991a). Molecular characterisation of a deletion encompassing the *Splotch* mutation on mouse chromosome 1. *Genomics* **10,** 89–93.

Epstein, D. J., Vekemans, M., and Gros, P. (1991b). *Splotch* (Sp^{2H}), a mutation affecting development of the mouse neural tube, shows a deletion within the paired homeodomain of *Pax3*. *Cell* **67,** 767–774.

Epstein, D. J., Vogan, K. J., Trasler, D. G., and Gros, P. (1993). A mutation within intron 3 of the *Pax3* gene produces aberrantly spliced mRNA transcripts in the *Splotch* (*Sp*) mouse mutant. *Proc. Natl. Acad. Sci. USA* **90,** 532–536.

Foy, C., Newton, V., Wellesley, D., Harris, R., and Read, A. P. (1990). Assignment of the locus for Waardenburg syndrome type I to human chromosome 2q37 and possible homology to the *Splotch* mouse. *Am. J. Hum. Genet.* **46,** 1017–1023.

Franz, T. (1989). Persistent truncus arteriosus in the *Splotch* mutant mouse. *Anat. Embryol.* **180,** 457–464.

Franz, T. (1990). Defective ensheatment of motoric nerves in the *Splotch* mutant mouse. *Acta Anat.* **138,** 246–253.

Franz, T. (1993). The *Splotch* (Sp^{1H}) and *Splotch*-delayed (Sp^{d}) alleles: Differential phenotypic effects on neural crest and limb musculature. *Anat. Embryol.* **187,** 371–377.

Galili, N., Davis, R. J., Fredericks, W. J., Mukhopadhyay, S., Rauscher, F. R., Emanuel, B. S., Rovera, G., and Barr, F. G. (1993). Fusion of a fork head domain gene to *PAX3* in the solid tumour alveolar rhabdomyosarcoma. *Nature Genet.* **5,** 230–235.

Godement, P., Vanselow, J., Thanos, S., and Bonhoeffer, F. (1987). A study in developing visual systems with a new method of staining neurones and their processes in fixed tissue. *Development* **101,** 697–713.

Goulding, M., Lumsden, A., and Paquette, A. J. (1994). Regulation of *Pax3* expression in the dermomyotome and its role in muscle development. *Development* **120,** 957–971.

Goulding, M., Sterrer, S., Fleming, J. Balling, R., Nadeau, J., Moore, K., Brown, S. D. M., Steel, K. P., and Gruss, P. (1993). Analysis of the *Pax3* gene in the mouse mutant. *Splotch. Genomics* **17,** 355–363.

Goulding, M. D., Chalepkis, G., Deutsch, U., Erselius, J. R., and Gruss, P. (1991). *Pax3*, a novel murine DNA binding protein expressed during early neurogenesis. *EMBO J.* **10,** 1135–1147.

Goulding, M. D., and Gruss, P. (1989). The homeobox in vertebrate development. *Curr. Opin. Cell. Biol.* **1,** 1088–1093.

Grim, M., Halata, Z., and Franz, T. (1992). Schwann cells are not required for guidance of motor nerves in the hindlimb in *Splotch* mutant mouse embryos. *Anat. Embryol.* **186,** 311–318.

Hamburger, V. (1961). Experimental analysis of the dual origin of the trigeminal ganglion in the chick embryo. *J. Exp. Zool.* **148,** 91–124.

Hatta, K., Takagi, S., Fujisawa, H., and Takeichi, M. (1987). Spatial and temporal expression pattern of N-cadherin cell adhesion molecules correlated with morphogenetic processes of chicken embryos. *Dev. Biol.* **120,** 215–227.

Hoth, C. F., Milunsky, A., Lipsky, N., Sheffer, R., Clarren, S. K., and Baldwin, C. T. (1993). Mutations in the paired domain of the human PAX3 gene cause Klein-Waardenburg syndrome (WSIII) as well as Waardenburg syndrome type I (WSI). *Am. J. Hum. Genet.* **52,** 455–462.

Ishikiriyama, S., Tonoki, H., Shibuya, Y., Chin, C., Harado, N., Abe, K., and Niikawa, N. (1989). Waardenburg syndrome type I in a child with de novo inversion (2) (q35q37.3). *Am. J. Hum. Genet.* **33,** 505–507.

Kessel, M. (1993). Reversal of axonal pathways from rhombomere 3 correlates with extra Hox expression domains. *Neuron* **10,** 379–393.

Kuratani, S. (1990). Development of the glossopharyngeal nerve branches in the early chick embryo with special reference to morphology of the Jacobson's anastomosis. *Anat. Embryol.* **181,** 253–269.

Kuratani, S., and Tanaka, S. (1990). Peripheral development of the avian vagus nerve with special reference to the morphological innervation of heart and lung. *Anat. Embryol.* **182,** 435–445.

Le Douarin, N. M. (1986). Cell line segregation during peripheral nervous system ontogeny. *Science* **231,** 1515–1522.

Lumsden, A., and Keynes, R. (1989). Segmental patterns of neuronal development in the chick hindbrain. *Nature* **337,** 424–428.

Maulbecker, C. C., and Gruss, P. (1993). The oncogenic potential of Pax genes. *EMBO J.* **12,** 2361–2367.

McKusick, V. A. (1992). "Mendelian Inheritance in Man." Johns Hopkins Univ. Press, Baltimore, MD.

Moase, C. E., and Trasler, D. G. (1989). Spinal ganglia reduction in the *Splotch*-delayed mouse neural tube defect mutant. *Teratology* **40,** 67–75.

Moase, C. E., and Trasler, D. G. (1990). Delayed neural crest emigration from Sp and Sp^d mouse neural tube explants. *Teratology* **42,** 171–182.

Moase, S. E., and Trasler, D. G. (1991). N-CAM alterations in *Splotch* neural tube defect mouse embryos. *Development* **113,** 1049–1058.

Moase, C. E., and Trasler, D. G. (1992). *Splotch* locus mouse mutants: Models for neural tube defects and Waardenburg syndrome type I in humans. *J. Med. Genet.* **29,** 145–151.

Noden, D. M. (1978). The control of avian cephalic neural crest cytodifferentiation. II. Neural tissues. *Dev. Biol.* **67,** 313–329.

Noden, D. M. (1993). Spatial integration among cells forming the cranial peripheral nervous system. *J. Neurobiol.* **24,** 248–261.

O'Shea, K. S., and Liu, L.-H. J. (1987). Basal lamina and extracellular matrix alterations in the caudal neural tube of the *delayed Splotch* embryo. *Dev. Brain Res.* **37,** 11–20.

Pantke, O., and Cohen, M. (1971). The Waardenburg syndrome. *Birth Defects* **7,** 147–152.

Püschel, A. W., Balling, R., and Gruss, P. (1991). Separate elements cause lineage restriction and specify boundaries of *Hox-1.1* expression. *Development* **112,** 279–287.

Shapiro, D. N., Sublett, J. E., Li, B., Downing, J. R., and Naeve, C. W. (1993). Fusion of *PAX3* to a member of the Forkhead Family of transcription factors in human alveolar rhabdomyosarcoma. *Cancer Res.* **53,** 5108–5112.

Simon, H., and Lumsden, A. (1993). Rhombomere-specific origin of the contralateral vestibulo-acoustic efferent neurons and their migration across the embryonic midline. *Neuron* **11,** 209–220.

Tassabehji, M., Read, A. P., Newton, V. E., Harris, R., Balling, R., Gruss, P., and Strachan, T. (1992). Waardenburg's syndrome patients have mutations in the human homologue of the *Pax3* paired box gene. *Nature* **355,** 635–636.

Tassabehji, M., Read, A. P., Newton, V. E., Patton, M., Gruss, P., Harris, R., and Strachan, T. (1993). Mutations in the *PAX3* gene causing Waardenburg syndrome type 1 and type 2. *Nature Genet.* **3,** 26–30.

Thiery, J. P., Duband, J. L., and Tucker, G. C. (1985). Cell migration in the vertebrate embryo: Role of cell adhesion and tissue environment in pattern formation. *Annu. Rev. Cell Biol.* **1,** 91–113.

Trasler, D. G., and Morris-Kay, G. (1991). Immunohistochemical localization of chondroitin and heparan sulfate in pre-spina bifida *Splotch* mouse embryos. *Teratology* **44,** 571–579.

Vogan, K. J., Epstein, D. J., Trasler, D. G., and Gros, P. (1993). The *Splotch-delayed* (Sp^d) mouse mutant carries a point mutation within the paired box of the *Pax3* gene. *Genomics* **17,** 364–369.

Waardenburg, P. (1951). A new syndrome combining developmental anomalies of the eyelids, eyebrows, and nose root with congenital deafness. *Am. J. Hum. Genet.* **3,** 195–253.

Walther, C., Guénet, J.-L., Simon, D., Deutsch, U., Jostes, B., Goulding, M., Plachov, D., Balling, R., and Gruss, P. (1991). Pax: A murine multigene family of paired box containing genes. *Genomics* **11,** 424–434.

Yang, X.-M., and Trasler, D. G. (1991). Abnormalities of neural tube formation in pre-spina bifida *Splotch*-delayed mouse embryos. *Teratology* **43,** 643–657.

Received for publication November 15, 1994
Accepted February 3, 1995